NANO · MICRO small
www.small-journal.com

Check for updates

Anisotropic Strain Relaxation of Graphene by Corrugation on Copper Crystal Surfaces

Bing Deng, Juanxia Wu, Shishu Zhang, Yue Qi, Liming Zheng, Hao Yang, Jilin Tang, Lianming Tong, Jin Zhang, Zhongfan Liu, and Hailin Peng**

Corrugation is a ubiquitous phenomenon for graphene grown on metal substrates by chemical vapor deposition, which greatly affects the electrical, mechanical, and chemical properties. Recent years have witnessed great progress in controlled growth of large graphene single crystals; however, the issue of surface roughness is far from being addressed. Here, the corrugation at the interface of copper (Cu) and graphene, including Cu step bunches (CuSB) and graphene wrinkles, are investigated and ascribed to the anisotropic strain relaxation. It is found that the corrugation is strongly dependent on Cu crystallographic orientations, specifically, the packed density and anisotropic atomic configuration. Dense Cu step bunches are prone to form on loose packed faces due to the instability of surface dynamics. On an anisotropic Cu crystal surface, Cu step bunches and graphene wrinkles are formed in two perpendicular directions to release the anisotropic interfacial stress, as revealed by morphology imaging and vibrational analysis. Cu(111) is a suitable crystal face for growth of ultraflat graphene with roughness as low as 0.20 nm. It is believed the findings will contribute to clarifying the interplay between graphene and Cu crystal faces, and reducing surface roughness of graphene by engineering the crystallographic orientation of Cu substrates.

Surface corrugation is a common phenomenon for heteroepitaxial growth of thin films on substrates, which is related to the stress-induced morphological instability due to the mismatch in mechanical properties, i.e., lattice mismatch or thermal mismatch.[1,2] This phenomenon is more obvious for epitaxial growth of graphene, the 2D crystal to the limitation of thickness, on metal substrates by chemical vapor deposition (CVD). The ultimate flexibility of graphene enables the growth of intact graphene layers on substrates which have large lattice mismatch with graphene.[3] However, the thermal mismatch-induced stress during cooling cannot be avoidable.

For graphene grown on Cu substrates, a temperature as high as ≈1000 °C is required for activating carbon precursors and initiating the growth. At this temperature, graphene is conformal with Cu substrates and free of stress. During cooling, the mismatch in thermal expansion coefficient between graphene (negative, $\alpha_{graphene} \approx -7 \times 10^{-6}$ K^{-1})[4,5] and Cu (positive, $\alpha_{Cu} = 18 \times 10^{-6}$ K^{-1}) induces strong thermal stress at the interface of graphene/Cu. This means two sides of a coin: Cu substrate is under tensile stress exerted by the thermal expansion of graphene, and graphene is under compressive stress exerted by the thermal contraction of Cu substrate. Accordingly, two correlative effects coexist: Cu undergoes surface roughening,[6–8] and graphene bulks to form wrinkles.[9,10] Upon transfer of graphene onto target substrates (e.g., SiO_2/Si), conventional methods cannot iron out the corrugated graphene conformal to the rough Cu substrates.[11,12] Hence, two types of surface roughness are ubiquitous: growth induced wrinkles,[13] and transfer induced nanoripples.[12] Graphene wrinkles can degrade mobility[13,14] and result in anisotropic electrical transport.[13,15] Hence, smoothing out graphene wrinkles to fabricate the ultraflat samples are highly required for improving the electrical performance.

To eliminate these wrinkles, it is necessary to reveal the key factors determining the corrugation process, including Cu surface roughening and graphene wrinkling. Many factors were proved to play a role, including sublimation of Cu at high temperature,[16] intrinsic flatness of Cu substrate,[17] crystalline orientation of Cu,[18] graphene layers,[6] and cooling rate.[19]

B. Deng, S. Zhang, Y. Qi, L. Zheng, H. Yang, J. Tang, Prof. L. Tong, Prof. J. Zhang, Prof. Z. Liu, Prof. H. Peng
Center for Nanochemistry (CNC)
Beijing Science and Engineering Center for Nanocarbons
Beijing National Laboratory for Molecular Sciences (BNLMS)
College of Chemistry and Molecular Engineering
Peking University
Beijing 100871, China
E-mail: zfliu@pku.edu.cn; hlpeng@pku.edu.cn
Dr. J. Wu
CAS Key Laboratory of Standardization and Measurement for Nanotechnology
CAS Center for Excellence in Nanoscience
National Center for Nanoscience and Technology
Beijing 100190, P. R. China
Y. Qi, H. Yang
Academy for Advanced Interdisciplinary Studies
Peking University
Beijing 100871, China
Prof. J. Zhang, Prof. Z. Liu, Prof. H. Peng
Beijing Graphene Institute (BGI)
Beijing 100094, China

DOI: 10.1002/smll.201800725

 © 2018 WILEY-VCH Verlag GmbH & Co. KGaA, Weinheim

Considering the distinct atomic configurations of Cu crystal surfaces, both strain level and direction are different for graphene grown on them. Recently, a few groups have reported that graphene grown on Cu(111) can be free of wrinkle due to the strong interfacial coupling[20] or large friction force[21] between graphene and Cu(111). However, the detailed corrugation process of graphene on various Cu crystal surfaces, including the existence and extent of step bunches, the distribution of graphene wrinkles, and their relationship for the strain relaxation, are not fully revealed.

Here, the corrugation phenomena of graphene grown on Cu crystal faces were investigated and ascribed to anisotropic strain relaxation. We found that Cu surface deformation induced by releasing thermal stress was highly related to the packed density and atomic configuration of Cu substrates. For Cu(111) as the closest packed crystal face, the surface roughening was ignorable; in contrast, for loose packed Cu crystal faces, including Cu(100) and Cu(110), nanoscale periodic step bunches formed on the surfaces. This difference was attributed to the surface stability depending on the packed density of Cu crystal faces. On a loose packed Cu surface, anisotropic strain relaxation was observed: dense Cu step bunches formed along the loose packed lattice direction of Cu, and graphene wrinkles formed by delaminating from Cu in the perpendicular direction. Surface roughening is an effective way to release strain. Therefore, the remaining strain of graphene on corrugated Cu crystal surfaces is smaller than that on flat surfaces. The strain difference may account for the variation in oxidation behavior of graphene coated Cu crystal faces. Our findings will contribute to interpreting the interplay between graphene and Cu crystal faces, and engineering Cu substrates for ultrasmooth graphene growth.

The relevance of Cu surface roughening with crystallographic orientation of Cu was revealed combining scanning electron microscopy (SEM) and electron back scattering diffraction (EBSD). The SEM image of graphene grown on Cu using low pressure CVD showed two types of roughness features (**Figure 1**a), that is, periodic CuSB (red arrows) and linear graphene wrinkles (yellow arrows). According to the EBSD image at the same region (Figure 1b), the correlation between Cu crystallographic orientations and CuSB was revealed. Except the flat Cu(111) crystal face, obvious CuSB with varied degree and orientation existed on other crystal faces, including Cu(100), Cu(110) (Figure 1a), and other high-index crystal faces (Figure S3, Supporting Information). In addition, graphene wrinkles can cross over Cu grain boundaries and existed on all crystal surfaces (Figure 1a). More interestingly, on a specific Cu domain, the distribution of CuSB and graphene wrinkles was anisotropic. The isolated wrinkles were roughly vertical to the densely aligned CuSB, as identified by both SEM (Figure 1c; and Figure S4a, Supporting Information) and atomic force microscopy (AFM) images (Figure 1d; and Figure S4b, Supporting Information). The width and height of the wrinkle in Figure 1d were about 20 and 0.6 nm, respectively, indicating the folded structure.[13]

The correlation between Cu surface roughening and Cu crystal faces is explained by Cu surface dynamics. The corrugation process of graphene on Cu is illustrated in Figure 1e,f. When Cu is heated up to the temperature near its melting point (T_m), some outmost surface atoms become "quasiliquid" due to surface premelting.[22–25] This phenomenon was in situ observed by environmental SEM (ESEM) during graphene growth on Cu.[26] The surface premelting is related to the crystallographic orientation: the surface stability of Cu crystal faces against disordering follows the order of packed density.[23] The atomic configurations of Cu(111), Cu(100), Cu(110), and Cu(103) are shown in Figure S5 (Supporting Information). As the closest packed crystal face, Cu(111) keeps crystalline state up to T_m = 1084 °C.[23] Other low-index crystal faces of Cu(100) and Cu(110), and high-index faces undergo surface premelting with varied initiated temperature and thickness of premelting layer.[27] During cooling in the CVD process, the thermal mismatch between Cu and graphene induces strong tensile strain on Cu surfaces.[6,7] As a result, the Cu surface underwent surface roughening by solidifying the premelting layer. In the case of Cu(111) without premelting layer, the stress exerted by graphene might be not large enough to induce obvious surface reconstruction. Hence, Cu(111) is the best crystal face for step bunch-free and ultrasmooth graphene growth.

The orientation of Cu step bunches depends on the lattice direction of underlying Cu crystal faces. In particular, the orientation of CuSB is the same inside a Cu domain (Figure 1a; and Figure S6, Supporting Information), and varied across the Cu grain boundaries (Figure 1a; and Figure S7, Supporting Information). Surface roughening of Cu(100) was investigated to clarify the orientation relationship between CuSB and Cu lattice direction. A Cu domain was verified to be (100)-oriented by EBSD (**Figure 2**a). SEM image of the same region showed isolated graphene islands aligned in two perpendicular directions (Figure 2b), consistent with previous statement that graphene nucleated along the directions of Cu[110] and Cu[$\bar{1}$10] on a Cu(100) substrate.[28,29] The orientation of CuSB beneath different graphene islands were the same independent of the lattice direction of graphene (Figure 2c). The AFM image of the Cu(100) surface showed the atomic steps in two perpendicular orientation (Figure 2d), corresponding to the lattice vectors of [110] and [$\bar{1}$10]. This is because Cu(100) crystal face is fourfold symmetry, and tends to form atomic steps along lines where the slip planes reach the surface. The AFM image at the edge region of a graphene island on Cu(100) showed that the CuSB was roughly parallel to one direction of Cu atomic steps (Figure 2e). Hence, we conclude that the CuSB is formed along the direction of Cu[110] (or [$\bar{1}$10]) and independent of graphene lattice orientation. As schematically shown in Figure 2f, under tensile stress exerted by graphene during cooling, the premelting layer on Cu surface solidified along the glide plane to enlarge the surface due to the feasibility of deformation along this direction (Figure S5b, Supporting Information).

The above analysis for CuSB formation on Cu(100) can be generalized to other anisotropic crystal faces, such as Cu(110). The CuSB on Cu(110) was parallel to the long axis of graphene islands, which is also the lattice direction of Cu[$\bar{1}$01] (Figure S8, Supporting Information). This is because Cu(110) crystal face is twofold symmetry, and tends to reconstruct along the lattice direction of [$\bar{1}$01] (Figure S5c, Supporting Information). In sharp contrast, Cu(111) is a crystal face with sixfold symmetry, and can form atomic steps in the directions of [110], [101], and [001] (Figures S5a and S9c, Supporting Information). Most

© 2018 WILEY-VCH Verlag GmbH & Co. KGaA, Weinheim

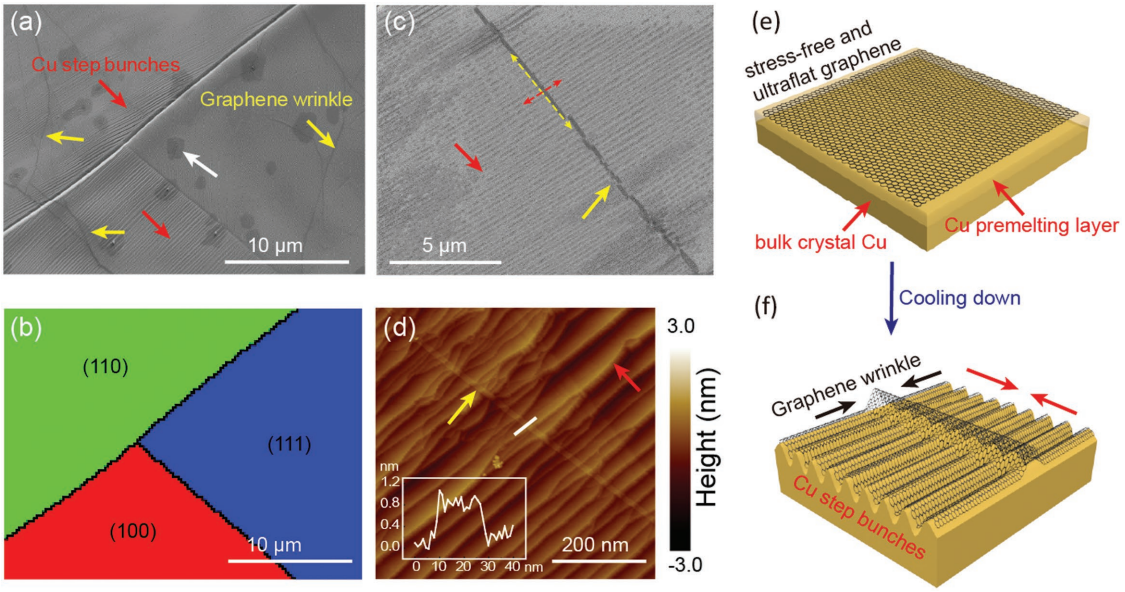

Figure 1. Corrugation of graphene grown on Cu substrates. a) SEM and b) EBSD images of graphene grown on polycrystalline Cu foil. The red, yellow, and white arrows showed Cu step bunches, graphene wrinkles, and graphene adlayers, respectively. c) SEM image of a graphene wrinkle. d) AFM image of a graphene wrinkle. Inset shows the line profile along the white line. e) Schematic of ultraflat graphene on Cu with a premelting layer. f) Schematic of the corrugation process during cooling. The black and red arrows indicated the buckling of graphene and the surface roughening of Cu, respectively.

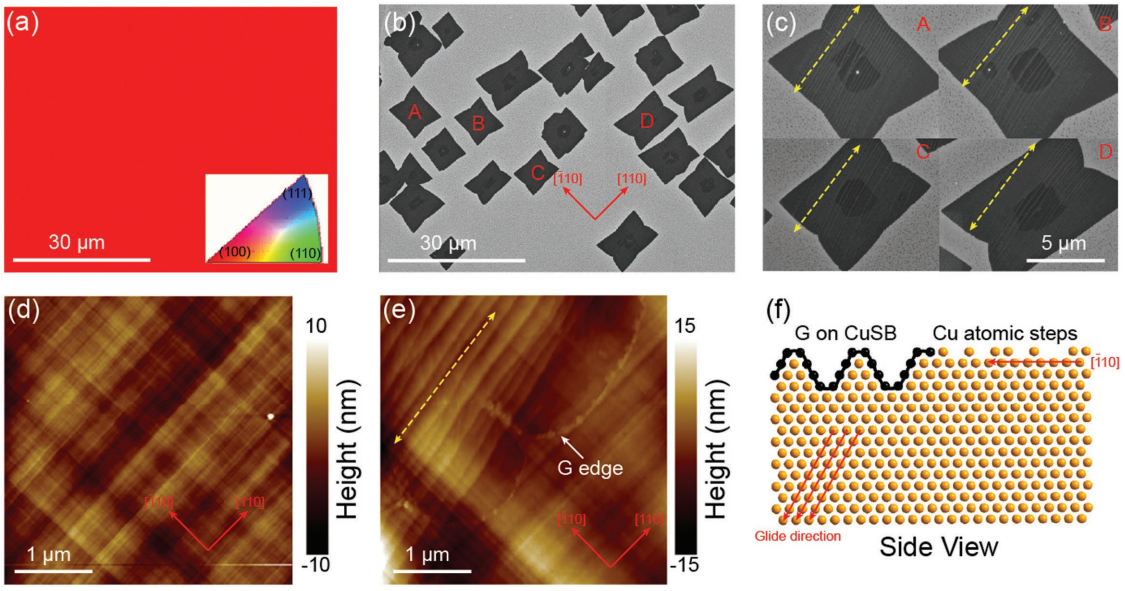

Figure 2. Surface roughening of Cu(100) under the tensile stress of graphene. a) EBSD image of a Cu domain, showing the (100)-orientation. b) SEM image of graphene islands at the same region in (a). c) Enlarged SEM images of graphene domains in (b). d) AFM image of Cu(100) face. e) AFM image of a graphene edge on Cu(100). The yellow arrow shows the orientation of CuSB. f) Schematic of side view of Cu step bunches and intrinsic Cu steps. The red lines shows the glide plane of Cu.

importantly, Cu(111) is the closest packed crystal face with nearly negligible premelting behavior,[28,30] so the tensile stress exerted by graphene does not induce obvious step bunching behavior (Figure S9d–f, Supporting Information). As a result, graphene grown on Cu(111) is very flat with the root-mean-square (RMS) roughness as low as 0.20 nm.

The distinct surface reconstruction behaviors among Cu crystal faces may affect the remaining strain of graphene layers.[6] We quantitatively investigated the correlation between Cu surface roughness and remaining strain of graphene by combining morphology imaging and vibrational analysis. As indicated in **Figure 3**a, the flat Cu domain and rough Cu domain were separated by a deep Cu grain boundary groove.[22] The as-grown graphene was monolayer to exclude the effect of layers on the surface roughening and strain relaxation[6] (Figure S10, Supporting Information). Figure 3b illustrated the height profiles on the flat and rough Cu domain. Line F was very flat; in contrast, Line R showed that the CuSB was roughly periodic

© 2018 WILEY-VCH Verlag GmbH & Co. KGaA, Weinheim

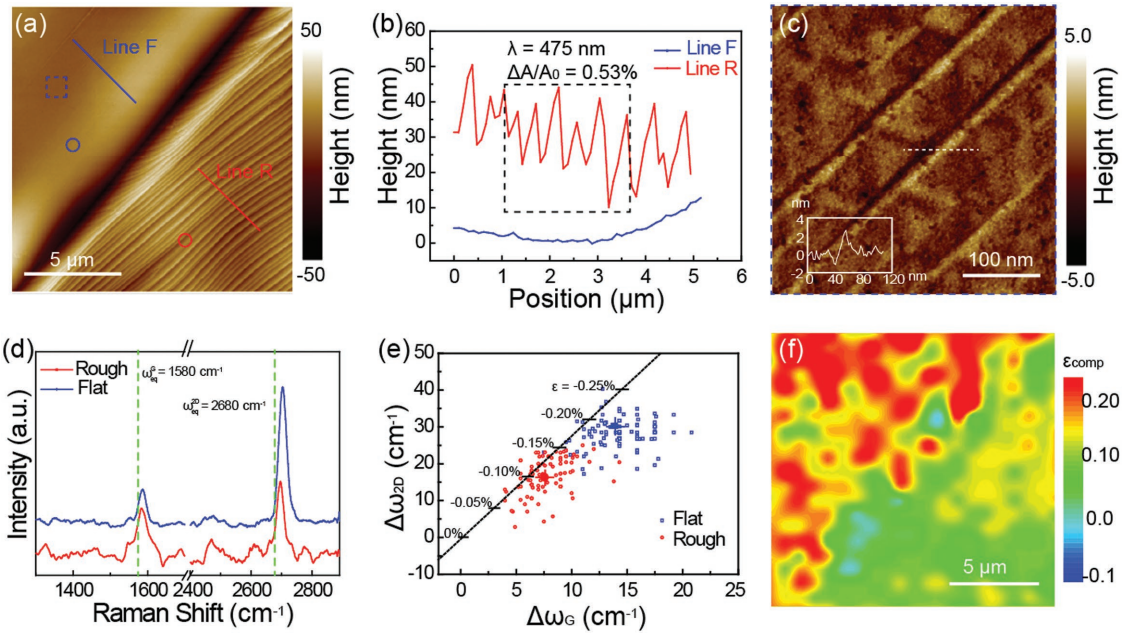

Figure 3. Strain relaxation of graphene by Cu surface roughening. a) AFM image of graphene covered Cu crystal faces with distinct roughness. b) AFM height profiles of flat and rough region in (a). c) Enlarged AFM image of the blue dashed area in (a). Inset shows the height profile of the white line. d) Raman spectra of the red and blue spots in (a). e) $\Delta\omega_{2D}$–$\Delta\omega_G$ correlation of the graphene in (a). The dashed line indicated the charge neutral line. f) Compressive strain distribution mapping of the region in (a).

with height of ≈20 nm and wavelength of ≈475 nm. Accordingly, the expansion ratio of the surface area of the rough Cu domain compared to the hypothetically flat plane was about 0.53%, and the increased area on the flat Cu domain was ignorable. The flat Cu domain underwent tiny surface reconstruction with Ra at ≈0.56 nm (Figure 3c). The line profile showed that the largest reconstruction step on flat Cu domain is mere 2 nm on the flat Cu domain, much smaller than that on the rough Cu domain. The difference in surface reconstruction between the two domains was ascribed to the distinct surface stability of Cu crystal surfaces.

Raman spectrum is widely used to investigate the strain and doping effect of graphene.[30–32] These two effects can be separated by correlated analysis of G and 2D bands, since the ratio of the shift of ω_{2D} and ω_G ($\Delta\omega_{2D}/\Delta\omega_G$) is very different.[33] Biaxially strained graphene, either compressive or tensile, shows a much larger ratio of $(\Delta\omega_{2D}/\Delta\omega_G)\varepsilon^{biaxial}$[34,35] than that induced by charge doping.[33,36,37] The representative Raman spectra of graphene on flat and rough Cu domain were shown in Figure 3d. Both D and G bands blueshifted compared to those of the stress-free intrinsic graphene, which might be a coherent effect of both strain and doping effect. Neither G nor 2D peaks exhibited obvious splitting, indicating that biaxial strain is dominant in both Cu domains. To exclude the doping effect, we plotted $\Delta\omega_G$ and $\Delta\omega_{2D}$ graph (Figure 3e). The dashed line indicated the $(\Delta\omega_{2D}/\Delta\omega_G)$ without charge doping effect, which had a slope of 2.8.[34] The dot distribution indicated that the observed blueshifts of G and 2D bands were dominated by compressive strain. Note that the small deviation of plots away from the slope was ascribed to the charge doping from underlying Cu substrate or absorbents in air.[38] The dots measured from flat area mainly distributed at the upper right compared to these measured from rough area, which clearly proved that graphene on flat Cu domain was more compressively strained than that on rough Cu domain. The average biaxial compressive strain of graphene was ≈0.2% on the flat Cu domain, while the value on the rough Cu was ≈0.1%. The strain mapping derived from Raman spectra was shown in Figure 3f, well consistent with morphology imaging by AFM (Figure 3a). Hence, the Cu surface roughening contributed to releasing the thermal mismatch-induced strain, and a small remaining strain level was expected for graphene grown on corrugated Cu surfaces.

In addition, the formation of graphene wrinkles is the other path for strain relaxation. The relationship between these two approaches (i.e., Cu step bunches, graphene wrinkles) has not been revealed yet. The strain relief associated with wrinkles is demonstrated in **Figure 4**. Two parallel graphene wrinkles were present on the Cu surface and perpendicular to CuSB (Figure 4a). Raman spectra along the line scan (yellow line) were measured to show the strain variation between the two parallel wrinkles. In the position of wrinkles, the G band was a single Lorentz peak and the peak position showed a minimal (Figure 4b). Hence the strain was released in the vicinity of graphene wrinkles, consistent with the strain relaxation in CVD graphene grown on Co.[39] In contrast, in the positions away from wrinkles, the G band split into G^+ and G^- components, indicating the uniaxial (or nonequibiaxial) strain in graphene lattice (Figure 4b,c).[31] The average shift of G^+ and G^- bands in the regions away from wrinkles (i.e., the points between 3 and 14 μm) are ≈1702.2 cm^{-1} and ≈1583.78 cm^{-1}. Supposing the Grüneisen parameter of $\partial\omega_{G^+}/\partial\varepsilon \sim -31.7$ $cm^{-1}/\%$ and $\partial\omega_{G^-}/\partial\varepsilon \sim -10.8$ $cm^{-1}/\%$,[31] the measured G^+ and G^- bands corresponded to compressive uniaxial strain of ≈0.70% and ≈0.35%.

© 2018 WILEY-VCH Verlag GmbH & Co. KGaA, Weinheim

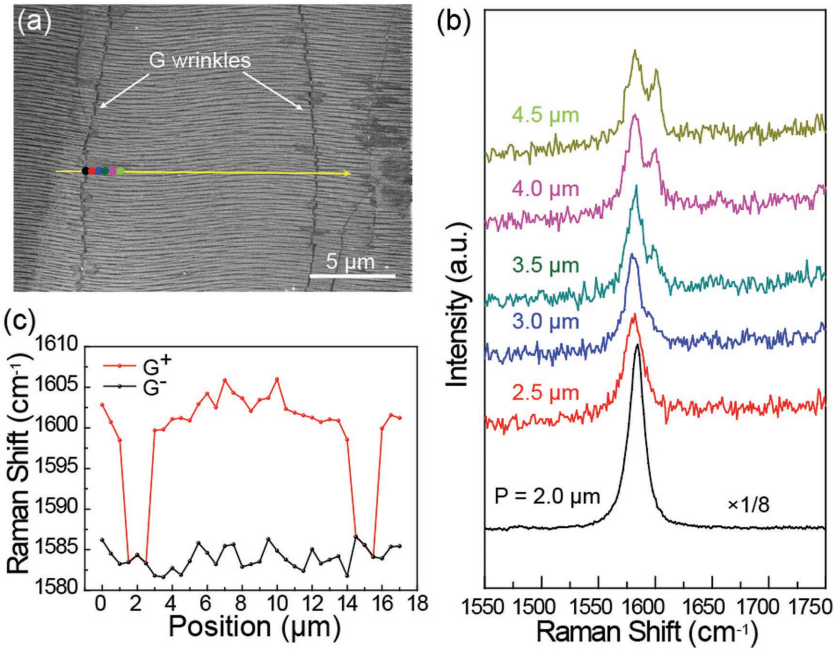

Figure 4. Strain variation around graphene wrinkles. a) SEM image of graphene grown on Cu(100) foil. b) Raman spectra of graphene on the spots in (a). c) Spatial variation in Raman G peak position along the arrow in (a).

Based on these observations, we can give a comprehensive interpretation about the corrugation at the interface of graphene/Cu substrates as the result of anisotropic strain relaxation (Figure 1e). At high temperature, the graphene grown on Cu substrates is ultraflat and stress-free. During cooling, thermal mismatch between graphene and Cu induce anisotropic stress on anisotropic Cu crystal faces. The premelting layer on Cu surface solidified according to its glide plane to form aligned Cu step bunches to release strain in this direction. The strain in the perpendicular direction cannot be released by surface roughening. As a result, graphene delaminated from the Cu substrate to form wrinkles once the accumulated strain overcame the active energy. Moreover, the surface roughening is an approach for global strain relaxation; in contrast, the graphene wrinkles can only release the strain in very vicinity.

The strain state of graphene grown on polycrystalline Cu is inhomogeneous and strongly correlated with Cu crystal faces, step bunches and wrinkles. The nonuniform strain may influence the properties of graphene. Here, we investigated the oxidation behavior of Cu covered by graphene under different strain fields. Graphene is impermeable to any molecules and has the potential as a perfect anticorrosion barrier. However, whether graphene can protect the underlying Cu substrates against oxidation is still under debate.[40–43] The as-grown graphene on Cu was stored in air for 1 week, and then characterized about the surface oxidation using SEM and Auger electron spectroscopy (AES). We found that the oxidation of Cu was initiated from the position of graphene wrinkles (**Figure 5**a). A nanochannel was supposed to form in the position of wrinkles. Hence, oxygen and water molecules might penetrate into the interface between graphene and Cu from the wrinkles to initiate the oxidation process.[40,44] Moreover, we found that the oxidation of Cu had a strong correlation with the surface roughness. The surfaces with abundant CuSB were preferential to be oxidized, while the flat Cu domain kept the intrinsic state (Figure 5b,c). As mentioned above, the graphene on rough Cu crystal faces was relaxed to a less strained state, which corresponded to a large delamination and a weak interfacial interaction. Hence, the relaxed interface facilitated oxygen and water molecules diffusion on the rough crystal faces to accelerate the oxidation process.[40,45]

In conclusion, the corrugation phenomena at the interface of graphene and Cu, including Cu surface roughening and graphene wrinkling, were attributed to the anisotropic thermal strain relaxation. The Cu surface roughening is highly correlated to Cu crystallographic orientations due to the distinct packed density and anisotropic atomic configuration. Cu(111) is the most stable crystal face with the least surface reconstruction. Hence, graphene grown on Cu(111) is ultrasmooth with roughness as low as 0.2 nm. On loose packed Cu crystal surfaces, on the other hand, aligned Cu step bunches and graphene wrinkles formed in perpendicular directions to release the anisotropic strain. Accordingly, the remaining strain of graphene on less corrugated Cu surface was larger, explaining the experimental observation that Cu was prone to oxidize on the rough crystal faces. A single crystal Cu(111) substrate is required for growing ultrasmooth and homogenously strained graphene films. Since the thermal mismatch-induced interfacial strain is common for

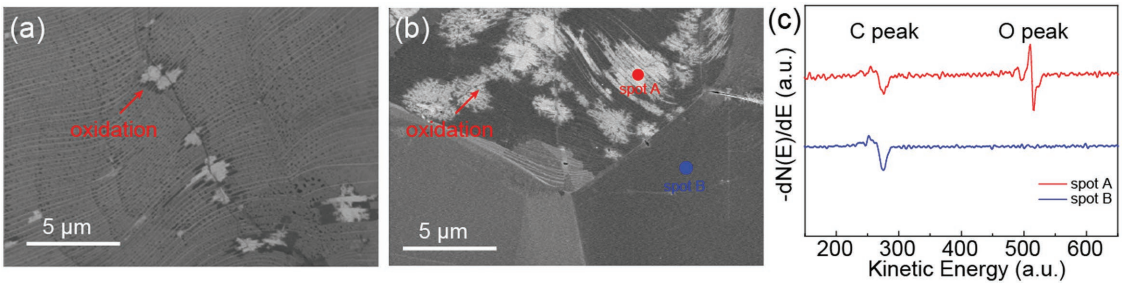

Figure 5. Oxidation behavior of Cu covered by graphene. a,b) SEM images of graphene/Cu after storage in air for one week. The white area indicated the oxidation of Cu. c) AES spectra of graphene covered Cu in the positions in (b).

© 2018 WILEY-VCH Verlag GmbH & Co. KGaA, Weinheim

hetero-epitaxial growth of materials, our findings may contribute to interpreting the corrugation of other 2D materials, such as *h*-BN.

Experimental Section

Graphene Growth: Commercially available rolled Cu foils (25 µm thick, 99% purity, Shanghai Zhonglv Corporation) were electrochemically polished in a electrolyte solution composed of phosphoric acid and ethylene glycol (V/V = 3:1) with a voltage of 2 V for 30 min. The Cu foil used for graphene growth was polycrystalline and atomically flat with Ra of ≈0.16 nm after electrochemical polishing (Figure S1, Supporting Information). Graphene growth was conducted in the hot center of a furnace (Lindberg/Blue M) equipped with a 1 in. diameter quartz tube. The system was first pumped to a base pressure of ≈5 Pa. Cu foil was annealed at 1045 °C in 100 sccm H_2 with pressure of ≈100 Pa for 30 min for annealing. After Cu annealing, the domain size of Cu enlarged to ≈100 µm, and the Cu domains remained atomically flat except the deep grain boundary grooves (Figure S2, Supporting Information). Then, 1 sccm CH_4 was introduced for 1–10 min for partially or fully covered graphene growth. After growth, graphene/Cu foil was rapidly cooled to room temperature at the speed of ≈200 °C min^{-1} without changing the gas flow. The as-synthesized graphene samples were characterized immediately after growth in avoid of oxidation.

Characterization: Optical microscopy images were collected on Nikon, Olympus LV100ND. SEM images were obtained on a Hitachi S4800 field-emission scanning electron microscope. EBSD measurements were carried out on AJEOLYSM-6500 F operated at 10 kV voltage with step size of 2 µm. AFM test was carried out on a Bruker Dimension Icon using the tapping mode. Confocal Raman measurements were performed on a JY Horiba HR800 Raman system with 514 nm (2.41 eV) line from an Ar^+ laser with laser spot size of 1 µm. The laser power on the sample was kept below 1 mW to avoid graphene heating. A 100 × objective and 600 lines mm^{-1} grating (spectral resolution was about 1 cm^{-1}) were used to collect Raman signal. AES was conducted on a ULVAX-PHI (PHI 710) Auger system, with the voltage of 10 kV and beam current of 10 nA.

Supporting Information

Supporting Information is available from the Wiley Online Library or from the author.

Acknowledgements

This work was financially supported by the National Basic Research Program of China (Nos. 2016YFA0200101 and 2014CB932500), the National Natural Science Foundation of China (Nos. 51432002, 51520105003, 21525310, 51672007, and 51502007), Beijing Municipal Science & Technology Commission (Nos. Z161100002116002 and Z161100002116021).

Conflict of Interest

The authors declare no conflict of interest.

Keywords

chemical vapor deposition, Cu, graphene, strain relaxation, wrinkles

Received: February 22, 2018
Revised: March 26, 2018
Published online: May 2, 2018

[1] H. J. Gao, W. D. Nix, *Annu. Rev. Mater. Sci.* **1999**, *29*, 173.
[2] C. S. Ozkan, W. D. Nix, H. J. Gao, *J. Mater. Res.* **1999**, *14*, 3247.
[3] H. Tetlow, J. P. de Boer, I. J. Ford, D. D. Vvedensky, J. Coraux, L. Kantorovich, *Phys. Rep.* **2014**, *542*, 195.
[4] W. Z. Bao, F. Miao, Z. Chen, H. Zhang, W. Y. Jang, C. Dames, C. N. Lau, *Nat. Nanotechnol.* **2009**, *4*, 562.
[5] D. Yoon, Y. W. Son, H. Cheong, *Nano Lett.* **2011**, *11*, 3227.
[6] J. H. Kang, J. Moon, D. J. Kim, Y. Kim, I. Jo, C. Jeon, J. Lee, B. H. Hong, *Nano Lett.* **2016**, *16*, 5993.
[7] J. Tian, H. Cao, W. Wu, Q. Yu, N. P. Guisinger, Y. P. Chen, *Nano Lett.* **2012**, *12*, 3893.
[8] T. M. Paronyan, E. M. Pigos, G. G. Chen, A. R. Harutyunyan, *ACS Nano* **2011**, *5*, 9619.
[9] X. Li, W. Cai, J. An, S. Kim, J. Nah, D. Yang, R. Piner, A. Velamakanni, I. Jung, E. Tutuc, S. K. Banerjee, L. Colombo, R. S. Ruoff, *Science* **2009**, *324*, 1312.
[10] Y. Zhang, T. Gao, Y. Gao, S. Xie, Q. Ji, K. Yan, H. Peng, Z. Liu, *ACS Nano* **2011**, *5*, 4014.
[11] Z. H. Pan, N. Liu, L. Fu, Z. F. Liu, *J. Am. Chem. Soc.* **2011**, *133*, 17578.
[12] G. X. Ni, Y. Zheng, S. Bae, H. R. Kim, A. Pachoud, Y. S. Kim, C. L. Tan, D. Im, J. H. Ahn, B. H. Hong, B. Ozyilmaz, *ACS Nano* **2012**, *6*, 1158.
[13] W. J. Zhu, T. Low, V. Perebeinos, A. A. Bol, Y. Zhu, H. G. Yan, J. Tersoff, P. Avouris, *Nano Lett.* **2012**, *12*, 3431.
[14] R. S. Ma, Q. Huan, L. M. Wu, J. H. Yan, W. Guo, Y. Y. Zhang, S. Wang, L. H. Bao, Y. Q. Liu, S. X. Du, S. T. Pantelides, H. J. Gao, *Nano Lett.* **2017**, *17*, 5291.
[15] D. Y. Zhang, Z. Jin, J. Y. Shi, P. Ma, S. G. Peng, X. Y. Liu, T. C. Ye, *Small* **2014**, *10*, 1761.
[16] Z. J. Wang, G. Weinberg, Q. Zhang, T. Lunkenbein, A. Klein-Hoffmann, M. Kurnatowska, M. Plodinec, Q. Li, L. F. Chi, R. Schloegl, M. G. Willinger, *ACS Nano* **2015**, *9*, 1506.
[17] J. H. Mun, J. G. Oh, J. H. Bong, H. Xu, K. P. Loh, B. J. Cho, *Nano Res.* **2015**, *8*, 1075.
[18] D. W. Kim, J. Lee, S. J. Kim, S. Jeon, H. T. Jung, *J. Mater. Chem. C* **2013**, *1*, 7819.
[19] H. R. Zhang, Y. H. Zhang, B. Wang, Z. Y. Chen, Y. Q. Zhang, Y. P. Sui, G. H. Yu, Z. Jin, X. Y. Liu, *RSC Adv.* **2015**, *5*, 96587.
[20] B. Deng, Z. Pang, S. Chen, X. Li, C. Meng, J. Li, M. Liu, J. Wu, Y. Qi, W. Dang, H. Yang, Y. Zhang, J. Zhang, N. Kang, H. Xu, Q. Fu, X. Qiu, P. Gao, Y. Wei, Z. Liu, H. L. Peng, *ACS Nano* **2017**, *11*, 12337.
[21] B.-W. Li, D. Luo, L. Zhu, X. Zhang, S. Jin, M. Huang, F. Ding, R. S. Ruoff, *Adv. Mater.* **2018**, *30*, 1706504.
[22] A. A. Pakhnevich, S. V. Golod, V. Y. Prinz, *J. Phys. D Appl. Phys.* **2015**, *48*, 435303.
[23] H. Hakkinen, M. Manninen, *Phys. Rev. B* **1992**, *46*, 1725.
[24] M. Polcik, L. Wilde, J. Haase, *Phys. Rev. Lett.* **1997**, *78*, 491.
[25] C. S. Jayanthi, E. Tosatti, L. Pietronero, *Phys. Rev. B* **1985**, *31*, 3456.
[26] Z. J. Wang, G. Weinberg, Q. Zhang, T. Lunkenbein, A. Klein-Hoffmann, M. Kurnatowska, M. Plodinec, Q. Li, L. Chi, R. Schloegl, M. G. Willinger, *ACS Nano* **2015**, *9*, 1506.
[27] R. Kojima, M. Susa, *High Temp-High Press.* **2002**, *34*, 639.
[28] A. T. Murdock, A. Koos, T. Ben Britton, L. Houben, T. Batten, T. Zhang, A. J. Wilkinson, R. E. Dunin-Borkowski, C. E. Lekka, N. Grobert, *ACS Nano* **2013**, *7*, 1351.
[29] Y. Ogawa, B. S. Hu, C. M. Orofeo, M. Tsuji, K. Ikeda, S. Mizuno, H. Hibino, H. Ago, *J. Phys. Chem. Lett.* **2012**, *3*, 219.
[30] V. Yu, E. Whiteway, J. Maassen, M. Hilke, *Phys. Rev. B* **2011**, *84*, 205407.
[31] T. M. G. Mohiuddin, A. Lombardo, R. R. Nair, A. Bonetti, G. Savini, R. Jalil, N. Bonini, D. M. Basko, C. Galiotis, N. Marzari, K. S. Novoselov, A. K. Geim, A. C. Ferrari, *Phys. Rev. B* **2009**, *79*, 205433.

© 2018 WILEY-VCH Verlag GmbH & Co. KGaA, Weinheim

[32] J. Yan, Y. B. Zhang, P. Kim, A. Pinczuk, *Phys. Rev. Lett.* **2007**, *98*, 166802.
[33] J. E. Lee, G. Ahn, J. Shim, Y. S. Lee, S. Ryu, *Nat. Commun.* **2012**, *3*, 1024.
[34] F. Ding, H. X. Ji, Y. H. Chen, A. Herklotz, K. Dorr, Y. F. Mei, A. Rastelli, O. G. Schmidt, *Nano Lett.* **2010**, *10*, 3453.
[35] J. Zabel, R. R. Nair, A. Ott, T. Georgiou, A. K. Geim, K. S. Novoselov, C. Casiraghi, *Nano Lett.* **2012**, *12*, 617.
[36] M. Lazzeri, F. Mauri, *Phys. Rev. Lett.* **2006**, *97*, 266407
[37] S. Pisana, M. Lazzeri, C. Casiraghi, K. S. Novoselov, A. K. Geim, A. C. Ferrari, F. Mauri, *Nat. Mater.* **2007**, *6*, 198.
[38] O. Frank, J. Vejpravova, V. Holy, L. Kavan, M. Kalbac, *Carbon* **2014**, *68*, 440.
[39] M. S. Bronsgeest, N. Bendiab, S. Mathur, A. Kimouche, H. T. Johnson, J. Coraux, P. Pochet, *Nano Lett.* **2015**, *15*, 5098.
[40] C. W. Huang, R. J. Shiue, H. C. Chui, W. H. Wang, J. K. Wang, Y. H. Tzeng, C. Y. Liu, *Nanoscale* **2013**, *5*, 9626.
[41] X. Xu, D. Yi, Z. Wang, J. Yu, Z. Zhang, R. Qiao, Z. Sun, Z. Hu, P. Gao, H. Peng, Z. Liu, D. Yu, E. Wang, Y. Jiang, F. Ding, K. Liu, *Adv. Mater.* **2018**, *30*, 1702944.
[42] J. Kwak, Y. Jo, S. D. Park, N. Y. Kim, S. Y. Kim, H. J. Shin, Z. Lee, S. Y. Kim, S. Y. Kwon, *Nat. Commun.* **2017**, *8*, 1549.
[43] M. Schriver, W. Regan, W. J. Gannett, A. M. Zaniewski, M. F. Crommie, A. Zettl, *ACS Nano* **2013**, *7*, 5763.
[44] B. N. Chandrashekar, B. Deng, A. S. Smitha, Y. B. Chen, C. W. Tan, H. X. Zhang, H. L. Peng, Z. F. Liu, *Adv. Mater.* **2015**, *27*, 5210.
[45] Y. H. Zhang, H. R. Zhang, B. Wang, Z. Y. Chen, Y. Q. Zhang, B. Wang, Y. P. Sui, B. Zhu, C. M. Tang, X. L. Li, X. M. Xie, G. H. Yu, Z. Jin, X. Y. Liu, *Appl. Phys. Lett.* **2014**, *104*, 143110.

© 2018 WILEY-VCH Verlag GmbH & Co. KGaA, Weinheim